Inorganic Chemistry

Article

pubs.acs.org/IC

Strong Ferromagnetic Exchange Interactions in Hinge-like $Dy(O_2Cu)_2$ Complexes Involving Double Oxygen Bridges

Yumi Ida,[†,⊥] Soumavo Ghosh,[‡,⊥] Ashutosh Ghosh,[*,‡] Hiroyuki Nojiri,[*,§] and Takayuki Ishida[*,†]

[†]Department of Engineering Science, The University of Electro-Communications, Chofu, Tokyo 182-8585, Japan

[‡]Department of Chemistry, University College of Science, University of Calcutta, 92, A.P.C. Road, Kolkata 700009, India

[§]Institute for Materials Research, Tohoku University, Katahira, Sendai 980-8577, Japan

Supporting Information

ABSTRACT: Two trinuclear isomeric compounds, $[\{(Cu^{II}(salpn))(Me(CO)Me)\}_2Dy^{III}(NO_3)_3]$ (**1**) and $[\{Cu^{II}(salpn)\}_2Dy^{III}(H_2O)(NO_3)_3]\cdot MeOH$ (**2**), along with one polymeric compound, $\{[\{Cu^{II}(salpn)\}_2Dy^{III}(NO_3)_3bpy]\cdot MeOH\cdot H_2O\}_n$ (**3**), were synthesized using a metalloligand, $[Cu^{II}(salpn)]$, where H_2salpn and bpy stand for *N*,*N*′-bis(salicylidene)-1,3-propanediamine and 4,4′-bipyridine, respectively. Compounds **1** and **2** were selectively prepared with two solvents: the less polar acetone led to the exclusive crystallization of **1** with a *transoid* trinuclear architecture, while more polar solvent methanol provided sole construction of **2** with a *cisoid* trinuclear architecture. Compound **3** was prepared from **1** or **2** after bpy was introduced as a bridge. The Dy and Cu ions are doubly bridged with oxygen atoms, and the core DyO_2Cu skeletons are characterized by different "butterfly angles" of 140.9(1)°, 147.1(19)°, and 142.4(2)° for **1**, **2**, and **3**, respectively. We have examined the molecular structures and magnetic properties of **1**−**3** using high-frequency electron paramagnetic resonance (HF-EPR), magnetization, and magnetic susceptibility techniques. These compounds showed slow magnetization reversal in the measurements of alternating current magnetic susceptibility. We analyzed EPR frequency-field diagrams using an effective spin-Hamiltonian including only one doublet of Dy sublevels and found that the exchange couplings are ferromagnetic in all compounds. The exchange coupling parameters J_{Dy-Cu} of **1**, **2**, and **3** were determined as 2.25 ± 0.05, 1.82 ± 0.04, and 1.79 ± 0.04 K, respectively. These values are larger than those found in previous research using EPR analysis on $[Cu^{II}(L^A)(C_3H_6O)Dy^{III}(NO_3)_3]$ (H_2L^A = *N*,*N*′-bis(3-methoxysalicylidene)-1,3-diamino-2,2-dimethylpropane) and $[Dy^{III}L^B_2(NO_3)_2\{Cu^{II}(CH_3OH)\}_2](NO_3)(CH_3OH)$ (H_2L^B = 2,6-bis(acetylaceto)pyridine). The present result shows an advantage of doubly oxygen-bridged motifs to built strong ferromagnetic interactions between lanthanide and transition metal ions. We found that the exchange coupling strength is sensitive to the structural parameters such as bond angles, bond lengths, and butterfly angles. Precise determination of the exchange parameters would contribute to development of exchange-coupled 4f−3d heterometallic complexes.

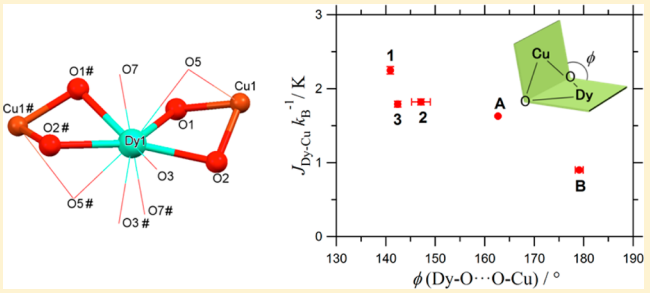

INTRODUCTION

Heterometallic 4f−3d compounds have been studied intensively for the development of single-molecule magnets (SMMs),[1−3] because lanthanide (Ln) ions have advantages of strong magnetic anisotropy and large magnetic moment.[4−6] The exchange coupling involved between 4f and 3d ions is one of the most important parameters to develop high-performance SMMs. The knowledge of the exchange coupling mechanism would be also useful for the development of bulk permanent magnets and refrigerants. In Gd−Cu systems, the ferromagnetic couplings between Gd^{3+} (S = 7/2) and Cu^{2+} (S = 1/2) are often observed;[7−10] for example, the dinuclear doubly oxygen-bridged Gd−Cu complexes have ferromagnetic couplings and show the S = 4 ground state.[11] In the case of Gd-based complexes, the exchange coupling can be evaluated by combining the temperature dependence of the magnetic susceptibility and the magnetization curve at low temperature. It is because Gd^{3+} is in the isotropic S-state, leading to simple analysis even with a powder sample. Moreover the consideration of the *LS* multiplet splitting is not necessary to analyze the magnetic data at low temperatures because the splitting is very large. Hence, the exchange couplings have been quantitatively studied by conventional magnetometries,[11−13] and their magneto−structure relation was well examined. It is noticed that a planar structure favors ferromagnetic coupling in the four-membered CuO_2Gd moiety. Although Gd^{3+} and Cu^{2+} ions are coupled ferromagnetically, there is a weak point of Gd complexes in developing new SMMs; Gd^{3+} ion has a spin-only character and weak magnetic anisotropy. It is a disadvantage compared with the heavy Ln ions having an unquenched orbital moment and large magnetic anisotropy.

Despite the clear advantages of using heavy Ln ions, there has been an essential difficulty in the determination of the

Received: July 15, 2015
Published: September 18, 2015

DOI: 10.1021/acs.inorgchem.5b01583
Inorg. Chem. 2015, 54, 9543−9555

Scheme 1. Structural Formulae of 1−3

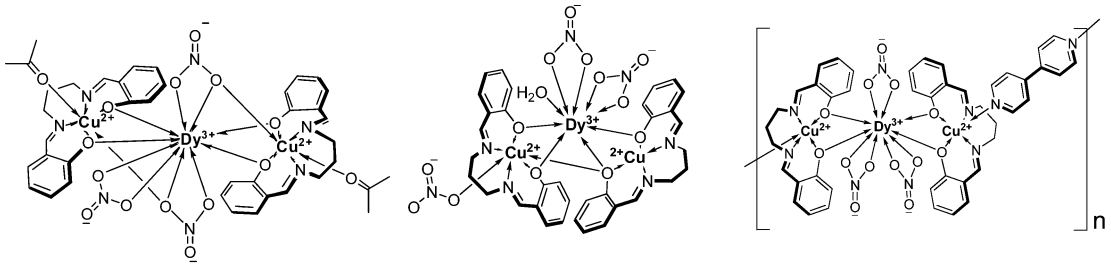

1 2 3

exchange couplings. An analysis of temperature dependence of the magnetic susceptibility is quite difficult because of the complex energy scheme caused by the spin−orbit coupling and crystal field splitting (CFS), and thus the exchange coupling parameter can hardly be determined by the magnetic susceptibility only.

We have developed a new microscopic method for the precise evaluation of exchange coupling in SMMs including heavy Ln ions[14−16] and have established their usefulness in the studies of various 4f−3d-based SMMs.[2,17] The key point is to use high-frequency electron paramagnetic resonance (HF-EPR) to observe the resonances of 3d transition metal ions biased by the exchange fields from Ln ions. The high magnetic field and low-temperature magnetization measurement, which traces the ground state of the system, is also combined with the EPR analysis. One of the most unique features of this method is that precise exchange couplings can be obtained even for powder specimens. It is because the different components can be distinguished by the *g* value, which is obtained by the slope of each mode in multiple-frequency EPR measurements. To generalize further this method, we would like to apply it to a series of 4f−3d heterometallic compounds with a small structural modification. The systematic work may afford a magneto−structure relation, which is highly important in research of 4f-based magnetic materials.

Taking the diphenoxo-bridged flexible dinuclear Cu−Tb motif, for example, it is found that when the Tb^{3+} ion is in a less symmetrical ligand field, it has easy-axis anisotropy and shows SMM behavior, but in a more symmetrical environment, the axial anisotropy is faded.[18] However, such studies are extremely rare in 4f−3d systems and to our knowledge only one such example is known. The paucity of such examples is presumably due to the lack of synthetic strategies using designed organic ligands allowing significant flexibility in the 4f−3d coordination clusters.[19] Recently, Ghosh et al. have shown that hinge-like coordination flexibility (*cisoid* and *transoid*; Scheme 1) can lead to the isolation of isomeric linear or bent structures for trinuclear $[\{M^{II}(salpn)\}_2M'(X)_2]$ (M and M′ are 3d metal ions) using a metalloligand $[M^{II}(salpn)]$ derived from a Schiff base H_2salpn (*N*,*N*′-bis(salicylidene)-1,3-propanediamine).[20] The different coordination environments of the central metal ion and bridging angles in these isomers brought about different magnetic behaviors such as "exchange coupling switch".[21] Very recently, we have evaluated the structure and the SMM property of a long-known but less-investigated family of $[\{Cu^{II}(salpn)\}_2Ln^{III}(X)_n]$ (Ln^{3+} = Tb^{3+}, a non-Kramers ion), where the flexible nature of metallatecton led to an interesting structural diversity.[22]

The motivation of the present work is to investigate the SMM behavior and 4f−3d exchange coupling in derivatives involving Ln^{3+} = Dy^{3+} (a Kramers ion) in different coordination environments but with the same ligand systems. We synthesized two solvates according to our synthetic strategy for isolation of linear and bent isomers of trinuclear 3d-metal ion complexes.[20] Herein, two trinuclear isomeric compounds, $[\{(Cu^{II}(salpn))(Me(CO)Me)\}_2Dy^{III}(NO_3)_3]$ (**1**) and $[\{Cu^{II}(salpn)\}_2Dy^{III}(H_2O)(NO_3)_3]\cdot MeOH$ (**2**), along with one polymeric compound, $\{[\{Cu^{II}(salpn)\}_2Dy^{III}(NO_3)_3bpy]\cdot MeOH\cdot H_2O\}_n$ (**3**), have been synthesized, where bpy stands for 4,4′-bipyridine (Scheme 1). Compounds **1** and **2** were selectively prepared by varying the solvent for synthesis. Compound **3** was derived from **1** or **2** on introducing bpy as a bridge between the trinuclear units. They possess a DyO_2Cu structure in common. The ferromagnetic coupling by direct current (dc) magnetic measurements and slow magnetization reorientation by alternating current (ac) magnetic susceptibility measurements for all complexes are also reported here.

The next motivation is to study the exchange coupling of a few new Dy−Cu compounds and compare the results on relevant compounds. The examination of relation between the exchange couplings and various structural parameters would be helpful for rational molecular design and synthesis of high-performance SMMs and related magnetic materials. To the best of our knowledge such systematic study of exchange coupling has not been made so far.

EXPERIMENTAL SECTION

Instruments. Elemental analyses (C, H, and N) were performed on a PerkinElmer 2400 series II CHN analyzer. IR spectra in KBr pellets (4000−500 cm^{-1}) were recorded on a PerkinElmer RXI FT-IR spectrophotometer. Powder X-ray diffraction patterns were recorded on a Bruker D-8 advance diffractometer operated at 40 kV and 40 mA and calibrated with a silicon standard, using monochromated Cu Kα (λ = 1.5406 Å) radiation.

Synthesis of Complex $[\{(Cu^{II}(salpn))(Me(CO)Me)\}_2Dy^{III}(NO_3)_3]$ (1). To a solution of [Cu(salpn)][23] (343.5 mg, 1.0 mmol) in 20 mL of acetone was added an acetone solution (5 mL) of $Dy(NO_3)_3\cdot 6H_2O$ (228.3 mg, 0.5 mmol). The resultant mixture was gently refluxed for 30 min. A dark green microcrystalline solid precipitate was separated on a filter and washed with cold acetone. A portion of the product was dissolved in acetone (5 mL) and slowly evaporated in a very long test tube at room temperature. After 2 days, well-shaped dark green crystals were precipitated. They were collected, washed, and dried under ambient atmosphere. The yield was 77%. Anal. Calcd for $C_{40}H_{44}N_7O_{15}Cu_2Dy$ (1152.42): C 41.69, H 3.85, N 8.51. Found: C 41.58, H 3.95, N 8.56%. IR: ν(C═O) = 1701 cm^{-1}, ν(C═N) = 1621 cm^{-1}, $\nu(NO_3^-)$ = 1553, 1279, and 1035 cm^{-1}.

Synthesis of Complex $[\{Cu(salpn)\}_2Dy(H_2O)(NO_3)_3]\cdot MeOH$ (2). To a solution of metalloligand [Cu(salpn)][23] (343.5 mg, 1.0 mmol) in methanol (15 mL) was added a methanol (5 mL) solution of $Dy(NO_3)_3\cdot 6H_2O$ (228.3 mg, 0.5 mmol). After being stirred at room temperature for 30 min, the mixture was filtered and kept for slow

DOI: 10.1021/acs.inorgchem.5b01583
Inorg. Chem. 2015, 54, 9543−9555

Table 1. Crystal Data and Structure Refinement Results for 1−3

compound	**1** (*transoid*)	**2** (*cisoid*)	**3** (polymeric)
formula	$C_{40}H_{44}N_7O_{15}Cu_2Dy$	$C_{35}H_{38}N_7O_{15}Cu_2Dy$	$C_{45}H_{46}N_9O_{15}Cu_2Dy$
formula weight	1152.42	1086.32	1242.49
crystal system	tetragonal	triclinic	monoclinic
space group	$I4_1/a$	$P\bar{1}$	$C2/c$
a, Å	17.583(5)	10.467(3)	15.334(6)
b, Å	17.583(5)	14.653(4)	25.950(10)
c, Å	29.716(5)	15.096(4)	15.975(9)
α, deg	90	104.450(3)	90
β, deg	90	100.006(3)	113.080(4)
γ, deg	90	99.252(3)	90
V, Å^3	9187(4)	2156.8(11)	5848(4)
Z	8	2	4
D_{cal}, g cm^{-3}	1.666	1.672	1.409
μ, mm^{-1}	2.601	2.764	2.050
R_{int}	0.0338	0.0487	0.0586
no. of unique data	4722	7419	5094
data with $I > 2\sigma(I)$	4057	5154	3606
R_1 on $I > 2\sigma(I)$[a]	0.0347	0.0650	0.0758
wR_2 (all data)[b]	0.0890	0.2245	0.2336
GOF on F^2	1.058	1.051	1.064

[a] $R_1 = \sum||F_o| - |F_c||/\sum|F_o|$. [b] $wR_2 = [\sum w(F_o^2 - F_c^2)^2/\sum w(F_o^2)^2]^{1/2}$.

Scheme 2. Synthesis of Complexes 1−3

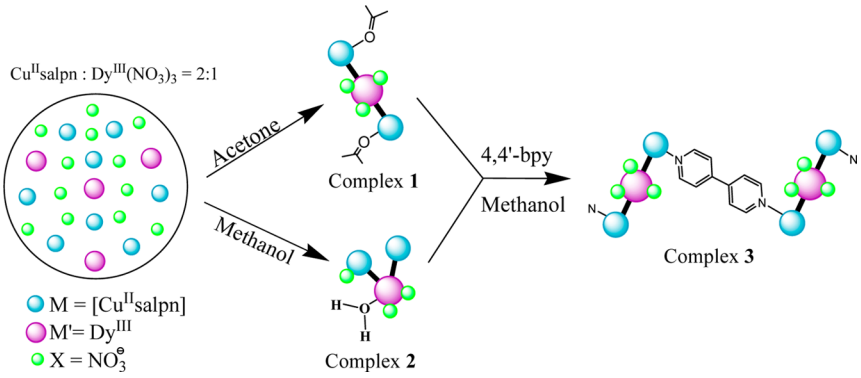

evaporation at room temperature. After 3 days, well-shaped dark green crystals were precipitated. They were collected, washed with a small amount of methanol, and dried under ambient atmosphere. The yield was 63%. Anal. Calcd for $C_{35}H_{38}N_7O_{15}Cu_2Dy$ (1086.32): C 38.70, H 3.53, N 9.03. Found: C 38.45, H 3.56, N 8.84%. IR: ν(C═N) = 1625 cm^{-1}, $\nu(NO_3^-)$ = 1555, 1284, and 1031 cm^{-1}.

Synthesis of [{Cu(salpn)}$_2$Dy(NO$_3$)$_3$bpy]·MeOH·H$_2$O}$_n$ (3). Compound **3** was prepared according to a method similar to that of the Tb analogue.[22] A solution of 4,4′-bipyridine (bpy, 50.0 mg, 0.32 mmol) in MeOH (1 mL) was added to a clear solution of **1** (368.8 mg, 0.32 mmol) or **2** (353.4 mg, 0.32 mmol) in MeOH (5 mL). After 3 days, light green block-shaped crystals were deposited. They were collected on a filter, washed with a small amount of methanol, and dried under ambient atmosphere. The yield was 64%. Anal. Calcd for $C_{45}H_{46}N_9O_{15}Cu_2Dy$ (1242.49): C 43.50, H 3.73, N 10.15%. Found: C 43.38, H 3.85, N 9.94%. IR: ν(C═N) = 1620 cm^{-1}, $\nu(NO_3^-)$ = 1560, 1281, and 1034 cm^{-1}.

Crystal Structure Analysis. Single crystals of **1**−**3** were mounted on a Bruker-AXS SMART APEX II diffractometer equipped with a graphite monochromator and Mo Kα radiation (λ = 0.71073 Å). The crystal was positioned at 60 mm distance from the CCD. Total 360 frames with an exposure time of 5 s were evaluated. The structure was solved using the Patterson method by using the SHELXS 97 program.[24,25] Non-hydrogen (H) atoms were refined with independent anisotropic displacement parameters. H atoms were placed at calculated positions, and their displacement parameters were fixed to be 1.2 times larger than those of the attached non-H atom, except for the interstitial water H atoms, which could not be located in the Fourier map. For **1** and **3**, there are large accessible voids, but there is no discernible electron density. Absorption corrections were carried out using the SADABS program.[26] All calculations were performed using SHELXS 97,[24] SHELXL 97,[25] PLATON 99,[27] ORTEP-32,[28] and WinGX system ver-1.64.[29] CCDC 1059357, 1059358, and 1050447 were assigned for **1**, **2**, and **3** respectively. Selected bond distances and bond angles for **1**−**3** are given in Table 1 and Tables S1−S3 (Electronic Supporting Information).

dc and ac Magnetic Measurements. The dc magnetic susceptibilities and magnetizations of polycrystalline specimens of **1**−**3** were measured on an MPMS-XL7 SQUID magnetometer (Quantum Design) in a temperature range of 1.8−300 K. The magnetization was measured in a field range of 0−7 T. Diamagnetic contribution from the sample holder was corrected with blank data measured separately. Diamagnetism of the sample itself was estimated from Pascal's constants.[30] Ac magnetic susceptibilities of **1**−**3** were measured on a PPMS model 6000 ac/dc magnetometer (Quantum Design) down to 1.9 K at zero dc field.

High-Frequency Electron Paramagnetic Resonance. HF-EPR spectra for polycrystalline samples of **1**−**3** were measured between 95 and 450 GHz at temperatures from 1.7 to 40 K by using the TESRA-P EPR spectrometer installed at Institute for Materials Research, Tohoku

DOI: 10.1021/acs.inorgchem.5b01583
Inorg. Chem. 2015, 54, 9543−9555

University.[31] The sample was packed in a case made of polyethylene. Gunn oscillators and backward traveling wave oscillators were used as radiation sources, and InSb was used as detector.[31]

RESULTS

Synthesis and Characterization. We have established that various factors (solvents, temperature etc.) can change the orientation of the metalloligands around the central metal ion to result in *transoid* or *cisoid* isomers or solvates.[20,21] In the present study, we have utilized our expertise in solvent-driven change of orientation of metalloligands around Dy^{3+}. A relatively nonpolar aprotic solvent like acetone helps to assemble *transoid* solvate **1**, whereas polar protic methanol assists the formation of *cisoid* solvate **2** as shown in Scheme 2. Other solvents, for example, ethanol and acetonitrile, also favored the formation of the *cisoid* complex. The phase purity of both **1** and **2** has been confirmed from identity of the powder X-ray diffraction (PXRD) patterns (Figure 1), indicating that

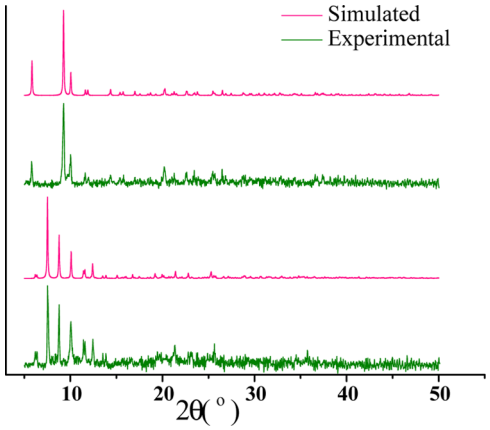

Figure 1. PXRD patterns of (top) **1** and (bottom) **2**.

each isomeric structure was formed exclusively. In addition to elemental and PXRD analyses, the complexes were further characterized by IR spectra. The precursor metalloligand [Cu(salpn)] does not have any counteranions, whereas the products contain nitrato coligands. The characteristic bands for bidentate chelation of nitrato anions in each compound were observed.[32] A strong and sharp band of the azomethine ν(C═N) group of the Schiff base appears at 1620−1625 cm^{-1} for **1** and **2**. A strong sharp peak at 1701 cm^{-1} for only **1** was observed due to the ν(C═O) group of the coordinated acetone molecules.

Complex **3** can be prepared by reacting either **1** or **2** with 4,4′-bipyridine in a methanol solution. Besides elemental analyses, the complex was characterized by IR spectra. The nitrato anion showed its characteristic bands for bidentate chelation.[23b] A strong and sharp band due to the azomethine ν(C═N) group remained at 1620 cm^{-1}.

Crystal Structures. Complexes **1**−**3** have the same [{Cu(salpn)}$_2$Dy] core skeleton, like a molecular hinge with *cisoid*−*transoid*-type folding.[20,21] The molecular structure of **1** together with atomic numbering is shown in Figure 2a. The space group of the crystal of **1** is tetragonal $I4_1/a$ with $Z = 8$. In the trinuclear molecule, two metalloligands [Cu(salpn)] serve as a chelate ligand to the central Dy^{3+} ion via bidentate μ_2-phenoxido oxygen atoms in approximately coplanar orientation, making the {Cu(salpn)}$_2$Dy coordination cluster *transoid*. In addition, three chelating nitrato (κ^2O,O') coligands are bonded to the Dy center, building up deca-coordination. Two of three nitrates also bridge ($1\kappa O{:}2\kappa^2O,O'$) the Cu atoms with the Dy centers. The molecule is symmetrically halved by a C_2 axis passing parallel to the crystallographic *c*-axis through the O4−N3−Dy1 atoms. Accordingly the nearest Dy···Cu geometry is unique, which will be important information for modeling of exchange coupling.

The vertex of the coordination polyhedron of the central Dy^{3+} ion in **1** is symmetrically constructed by 10 oxygen atoms from five bidentate ligands with average Dy−O bond distances of 2.51(1) Å that can be regarded as a distorted tetradecahedron.[34] Selected bond distances and angles are summarized in Table 2. Four oxygen atoms of the two metalloligands, that is, O1 and O2 (and $O1^{\#}$ and $O2^{\#}$), are at the distances of 2.368(3) and 2.372(2) Å, respectively, where the symmetry operation code of # is $1 - x, 1/2 - y, z$. Another four, that is, O5 and O7 (and $O5^{\#}$ and $O7^{\#}$), belonging to two nitrato coligands are at distances of 2.756(6) and 2.543(7) Å, respectively. The rest of them, that is, O3 (and $O3^{\#}$) belong to the symmetrically bidentate nitrate coordinated to Dy at a distance of 2.500(3) Å. Six oxygen atoms O2, O5, O7, $O2^{\#}$, $O5^{\#}$, and $O7^{\#}$ nearly form an equatorial plane, whereas O1, $O1^{\#}$ and O3, $O3^{\#}$ are located at the opposite side of this plane in such a manner that the O1−Dy1−$O1^{\#}$ plane bisects the angle O3−Dy1−$O3^{\#}$. The root-mean-square (rms) deviation of the six equatorial atoms from the mean plane passing through them is 0.281(10) Å with the Dy atom displaced by 0.026(1) Å.

Each of the two symmetrically related terminal copper atoms of the trinuclear [{Cu(salpn)}$_2$Dy] core in **1** is bonded to N_2O_2 donor atoms (O1, O2, N1, and N2 for Cu1) of the tetradentate ligand $salpn^{2-}$, making up the equatorial plane with Cu−O and Cu−N distances of 1.944(3)−1.952(3) and 1.958(3)−1.978(4) Å, respectively. Two axial positions of the distorted octahedral Cu1 atoms are occupied by oxygen atoms O5 and O8 of a bridging nitrato coligand and acetone solvate at the distances of 2.616(6) and 2.573(4) Å, respectively. The bridging atoms are O1, O2, and O5 and the O1 and O2 bridges are important for the exchange coupling because they are located at the equatorial sites of Cu1.

The space group of **2** is $P\bar{1}$ with $Z = 2$. The whole molecule is crystallographically independent. Two bidentate metalloligands are bonded to the central Dy atom in an asymmetric angular orientation via two μ_2-phenoxido oxygen atoms (Figure 2b) that can be regarded as *cisoid* coordination. Two chelating nitrato (κ^2O,O') and one coordinated water molecule build up the nona-coordination, approximately forming a tricapped trigonal prism.[22] The third nitrato ligand is coordinated axially to the Cu atom of one of the coordinated metalloligands.

The vertexes of the coordination polyhedron of the central Dy^{3+} ion in **2** are constructed by nine oxygen atoms with average Dy−O bond distances of 2.43(2) Å. The four of the nine oxygen atoms, namely, O1, O2, O3, and O4, that belong to the two metalloligands are at distances 2.337(7)−2.496(7) Å. Another four oxygen atoms belonging to two nitrato coligands, that is, O8, O10, O11, and O13, are at distances between 2.438(8) and 2.550(9) Å.

There are two independent copper ions and accordingly two independent nearest Dy···Cu geometries. Each of the two terminal copper atoms of the trinuclear [{Cu(salpn)}$_2$Dy] core in **2** is bonded to four donor atoms of the N_2O_2 Schiff base $salpn^{2-}$, making up a planar arrangement. The Cu−O and Cu−N distances are in the ranges of 1.915(7)−1.977(7) Å and 1.937(12)−1.985(9) Å, respectively. One of the axial

DOI: 10.1021/acs.inorgchem.5b01583
Inorg. Chem. 2015, 54, 9543−9555

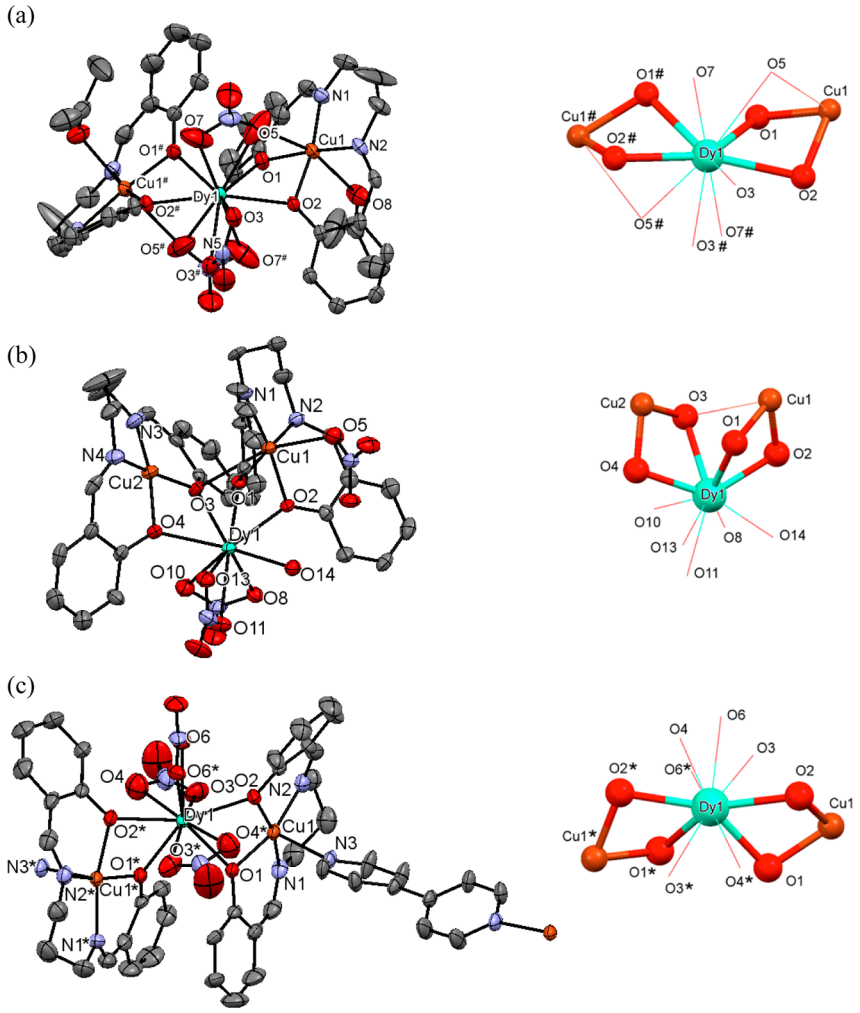

Figure 2. X-ray crystal structures (left) and skeletal views of the Dy surroundings and Cu atoms (right) for (a) **1**, (b) **2**, and (c) **3**. Thermal ellipsoids are drawn at the 30% probability level. Hydrogen atoms and solvent molecules are omitted for clarity. Atomic labeling of selected atoms is also shown. Symmetry operation codes of # in **1** and ∗ in **3** are $(1 - x, 1/2 - y, z)$ and $(1 - x, y, 1/2 - z)$, respectively.

Table 2. Selected Atomic Distances (Å), Bond Angles (deg), and Butterfly Angles (ϕ, deg)

	1	2	3
Dy1···Cu1	3.301(1)	3.311(2)	3.358(1)
Dy1···Cu2		3.356(2)	
Dy1−O1	2.368(3)	2.337(7)	2.376(6)
Dy1−O2	2.372(2)	2.385(7)	2.387(7)
Cu1−O1	1.944(3)	1.977(7)	1.976(6)
Cu1−O2	1.952(2)	1.959(7)	1.975(8)
Cu1−O3		2.802(8)	
Cu1−O5	2.616(6)	2.446(10)	
Dy1−O3	2.500(3)	2.496(7)	2.530(12)
Dy1−O7/O4[a]	2.543(7)	2.362(8)	2.606(14)
Cu2−O3		1.944(8)	
Cu2−O4		1.915(7)	
Cu1−O1−Dy1	99.5(1)	99.9(3)	100.6(2)
Cu1−O2−Dy1	99.1(1)	98.9(3)	100.3(3)
Cu2−O3−Dy1		97.4(3)	
Cu2−O4−Dy1		102.9(3)	
ϕ (Dy1−O1···O2−Cu1)	140.9(1)	148.9(3)	142.4(2)
ϕ (Dy1−O3···O4−Cu2)		145.2(3)	

[a]O7 for **1** and O4 for **2** and **3**.

coordination sites of Cu1 is occupied by an oxygen atom O5 of a nitrato coligand at a distance of 2.446(10) Å, indicating a square pyramidal geometry. Although Cu1 and Dy1 are triply bridged, the bond mediated by O3 does not contribute to Dy−Cu magnetic coupling because of the long bond length (2.802(8) Å). On the other hand, Cu2 has no axial ligand.

The intracluster Cu···Cu distances and Cu−Dy−Cu angles are 6.123(2) Å and 136.04(1)° and 3.725(2) Å and 67.94(4)° for **1** and **2**, respectively, indicating a closer orientation of the metalloligands in the latter. However, in the former, a large deviation of Cu−Dy−Cu angles from 180° indicates that the metal centers are not in a linear arrangement as found in heterometallic 3d−3d′−3d complexes.[20] One of the reasons could be an intramolecular $\pi-\pi$-stacking interaction via one pair of phenyl rings of the two metalloligands at the $C_g\cdots C_g$ distance of 3.777(4) Å with the dihedral angle of ca. 26.94° (C_g = centroid of the phenyl ring), which locks the molecular conformation to a nearly linear shape for this complex. The acetone molecules coordinated at copper atoms of **1** are inclined toward one of the phenyl rings of the Schiff base because of the intramolecular C−H(methyl)···π interaction. The distance between H(18A) and the centroid of the ring is 2.76 Å with the C−H···C_g angle of 136°.

DOI: 10.1021/acs.inorgchem.5b01583
Inorg. Chem. 2015, 54, 9543−9555

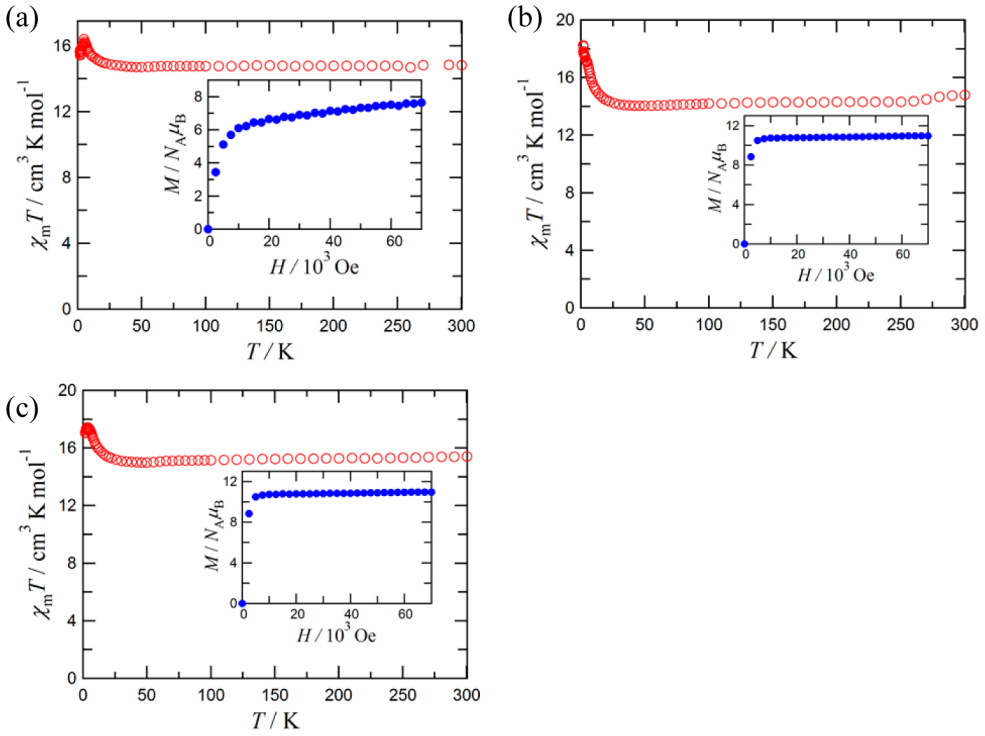

Figure 3. $\chi_m T$ vs T plots measured at 500 Oe for (a) **1**, (b) **2**, and (c) **3**. The insets show the magnetization curves measured at 1.8 K under nonfixed powder conditions.

There are very few reports of trinuclear complexes with various Ln ions and counteranions having either *cisoid* or *transoid* conformation.[35] Complexes **1** and **2** are the first example of *cisoid*–*transoid* [{Cu(salpn)}$_2$Dy] structural units constituting of the same Cu(salpn) and Ln. A polar protic solvent, methanol, facilitates the formation of **2** with a bent [{Cu(salpn)}$_2$Dy] unit (*cisoid*), whereas a relatively less polar aprotic solvent like acetone assists the linear arrangement of metalloligand in **1** (*transoid*). Such solvent induced *cisoid*–*transoid* changes in heterometallic 4f–3d coordination complexes are extremely rare and previously obtained by ligand-backbone modifications.[36] Among them, bicompartmental N_2O_4 donor ligands warrant a particular mention because they proved to be robust to attain desired oligonuclear complexes and coordination polymers.[37] However, in such cases, the central Ln locates in the 2 × O_2O_2' compartment (O1/O2 and O1$^{\#}$/O2$^{\#}$ in **1** or O1/O2 and O3/O4 in **2**), which makes the complex rather rigid, and mostly they are found in a *transoid* configurations. In some other analogous 4f–3d complexes, the relative orientation of the 3d ions with respect to the Ln ions also seems to be fixed.[38]

Compound **3** crystallizes in a monoclinic $C2/c$ space group with Z = 4 (Figure 2c). The molecules of **3** form an infinite chain along the crystallographic a axis with [{Cu(salpn)}$_2$Dy(NO$_3$)$_3$bpy] as a repeating unit. The asymmetric unit involves half of the repeating unit owing to the 2-fold symmetry; namely, the nearest Cu···Dy geometry is unique.

The repeating unit of **3** consists of a trinuclear core {Cu(salpn)}$_2$Dy(NO$_3$)$_3$ and a bpy bridge. The Dy^{3+} ion is ten-coordinate with four oxygen atoms from two [Cu(salpn)] and six oxygen atoms from three bidentate nitrate ions. The copper ion has a N_2O_2 donor set (O1, O2, N1, and N2) of the tetradentate ligand salpn on the basal plane. Although there is a bpy molecule between the nearest neighboring Cu···Cu ions, the nitrogen atoms in bpy are located at an axial position of the copper ion. Hence, Cu···Cu exchange coupling will be negligible.[39] In short, **3** has a polymeric crystal structure, but the magnetic structure is practically monomeric as a {Cu(salpn)}$_2$Dy(NO$_3$)$_3$ unit.

In the repeating unit of **3**, the vertex of the coordination polyhedron of the central Dy^{3+} ion is similar to that of **1**. A C_2 axis runs through the Dy^{3+} ion, and an average Dy–O bond distance is 2.48(3) Å. Six oxygen atoms, that is, O2, O3, O4, O2*, O3*, and O4*, form nearly an equatorial plane, whereas the O1, O1*, O6, and O6* atom set organized at the opposite side of this plane in such a manner that the O1–Dy1–O1* plane bisects the O6–Dy1–O6* angle. The rms deviation of the six equatorially coordinated atoms from the mean plane passing through them is 0.272(26) Å with the Dy atom displaced toward O1 and O1* by 0.100(1) Å.

The Cu1···O3 distance of 2.815(14) Å to the other axial position is too long to be considered as a bond. Therefore, the geometry of Cu1 can be considered as a square pyramid. The rms deviation of the four basally coordinated atoms from the mean plane passing through them is 0.022(17) Å with the metal atoms 0.201(1) Å for Cu1 from this plane toward the axially coordinated N3 atom of the bpy molecule. The Addison parameter of Cu1 is 0.04, indicating negligible distortion toward a trigonal bipyramid.[33]

To feature the skeleton of LnO$_2$Cu four-membered rings, a "butterfly" angle, ϕ, is proposed as an important parameter.[11−13] The "butterfly" angle is between the two planes (CuO$_2$ and LnO$_2$) involving the bridging oxygen atoms and each metal ion. In the Gd–Cu dinuclear systems examined in the ref 11, when the GdO$_2$Cu ring is more planar, ferromagnetic coupling is stronger. Table 2 shows important geometrical parameters including butterfly angles. In the present {Cu(salpn)}$_2$Dy compounds, the nearest neighboring Dy^{3+} and Cu^{2+} ions are

DOI: 10.1021/acs.inorgchem.5b01583
Inorg. Chem. 2015, 54, 9543−9555

always exchange-coupled through the double oxygen bridge with a "butterfly" skeleton. There are one, two, and one crystallographically independent Dy···Cu geometries in the unit cells of **1**, **2**, and **3**, respectively. Accordingly the exchange coupling parameters J_{Dy-Cu} are unique for **1** and **3**, while **2** has two independent J_{Dy-Cu} parameters.

Magnetic Properties. Polycrystalline specimens of **1**−**3** were subjected to magnetic susceptometry (Figure 3). The randomly oriented samples were fixed with a small amount of mineral oil. Here, the $\chi_m T$ vs T plots are drawn in a temperature range of 1.8−300 K, and the static field of 500 Oe was applied. The observed $\chi_m T$ values at 300 K were 14.8, 14.8, and 15.4 cm^3 K mol^{-1} for **1**, **2**, and **3**, respectively, which are close to the expected value 14.9 cm^3 K mol^{-1} from the sum of two paramagnetic Cu^{2+} ions (S = 1/2, g = 2) and one free Dy^{3+} ion (J = 15/2, g_J = 4/3) for every $\{Cu(salpn)\}_2Dy$ unit. On cooling, the $\chi_m T$ values increased for all cases, which indicates possible ferromagnetic coupling, and as the crystallographic analysis indicates, they are ascribable to the interactions between the nearest Dy^{3+} and Cu^{2+} ions. Intermolecular exchange couplings are negligible because the nonmonotonic behavior of susceptibility at the lowest temperature regions is possibly caused by such negligible couplings.

The powder data of the magnetization curves of **1**−**3** were obtained at 1.8 K after the specimens were fixed with a small amount of mineral oil (Figure S1, Electronic Supporting Information). Slow saturation behavior was found, indicating the relatively strong magnetic anisotropy. To obtain information on the ground J^z value, we measured the magnetizations of powdery specimens without mineral oil and allowed them to align in the applied field direction. Field alignment effect was confirmed by the increase of the magnetization in the successive measurement cycles. As shown in the inset of Figure 3a, the magnetization of **1** is 7.6 μ_B at 7 T, and it is still gradually increasing. It indicates that the magnetic field alignment is not perfect. The finite slope of the magnetization curve in a higher magnetic field region is consistent with the partial orientation. Owing to the molecular arrangement in the tetragonal $I4_1/a$ space group, there are four different easy axis orientations in a unit cell. Because of the strong anisotropy of Dy^{3+}, the moments are canted from the external uniform magnetic field direction. This canting causes the large reduction of the saturation moments and almost linear increase in the high magnetic field side for **1**. Such behavior could not be observed for **2** or **3**, being incompatible with the unique magnetic easy axis in a unit cell owing to the crystallographic centrosymmetry.

The magnetization of **2** displayed more rapid saturation and reached the value of 11.0 μ_B at 7 T (the inset of Figure 3b). The saturation magnetization for ferrimagnetic configuration is 8 μ_B, and the ferromagnetic configuration is 12 μ_B when the g value of Cu^{2+} is 2 and J^z = ±15/2 for Dy^{3+} ion. Although the observed value was slightly smaller than 12 μ_B for the incomplete field alignment, the larger saturation value clearly indicates the presence of ferromagnetic coupling between Cu^{2+} and Dy^{3+} and the domination of the ground J^z = ±15/2 state for the Dy^{3+} ion in **2**.

We can also find a sharp rise of magnetization and the saturation moment of 11.0 μ_B per the formula unit for **3** (the inset of Figure 3c). The saturation moment is close to the theoretical 12 μ_B. Similarly to the case of **2**, the susceptibility and magnetization indicates that Dy^{3+} and Cu^{2+} couple ferromagnetically and that J^z = 15/2 is dominant in the ground state of Dy^{3+}.

However, we have to note that the perfectness of the magnetic field alignment is determined by the relation between the domain and powder sizes of the sample. A reduction is expected when the powder size is larger than the single domain size to give polycrystalline. Thus, the bulk measurement alone cannot provide a conclusion about the magnetic coupling and the ground state, and EPR measurement is essential for the quantitative analysis (see below).

The results on dc magnetic measurements are summarized in Table 3. The exchange couplings of the present Dy−Cu derivatives probably are all ferromagnetic. Many butterfly GdO_2Cu compounds showed ferromagnetic coupling.[11−13] According to an empirical rule,[8,15−17,22,40] the sign of the exchange coupling among Gd and heavy Ln ions are common in many cases. The present results are reasonably acceptable.

Table 3. Magnetic Properties of 1−3

	1	2	3
$\chi_m T$, cm^3 K mol^{-1} at 300 K	14.8	14.8	15.4
theoretical $\chi_m T$,[a] cm^3 K mol^{-1}	14.9	14.9	14.9
$\chi_m T$, cm^3 K mol^{-1} at 3 K	15.8	17.5	17.4
applied magnetic field, Oe	500	500	500
M, μ_B at 7 T, 1.8 K	7.6	11.0	11.0
theoretical saturation M,[b] μ_B	12	12	12

[a]Sum of free ion values; one J = 15/2 (Dy^{3+}) and two S = 1/2 (Cu^{2+}) ions. [b]Sum of the values from one J^z = 15/2 (Dy^{3+}) and two S = 1/2 (Cu^{2+}) ions.

Relaxation of Magnetization. The ac magnetic susceptibilities of powder specimens of **1**−**3** were measured at frequencies ν = 10−10000 Hz in T = 1.9−20 K (Figure 4). Below ca. 10 K, χ' decrease and concomitant χ'' increase were observed, especially for **2** and **3**, and their positions were shifted to a higher temperature on increasing frequency. The frequency dependence of the χ'' peak temperature can be analyzed by the Arrhenius law;[41] namely, the plots of the natural logarithm of the relaxation time, τ, evaluated by $1/(2\pi\nu)$ vs the inverse of the χ'' peak temperature, T eq 1. However, owing to the absence of χ'' peaks in the data of **1** (Figure 4a), a modified Arrhenius equation, eq 2, was applied to the analysis.[42]

$$\ln(2\pi\nu) = -\ln(\tau_0) - U_{eff}/(k_B T) \quad (1)$$

$$\ln(\chi''/\chi') = \ln(2\pi\nu\tau_0) + U_{eff}/(k_B T) \quad (2)$$

The modified Arrhenius plot for **1** and Arrhenius plots for **2** and **3** are shown in the insets of Figure 4. The effective energy barriers, U_{eff}, of the magnetization reversal and pre-exponential factors, τ_0, were calculated to be U_{eff}/k_B = 2.4 ± 0.6, 13.0 ± 0.2, and 11 ± 1 K and τ_0 = (3.6 ± 0.1) × 10^{-7}, (6.9 ± 0.5) × 10^{-7}, and (1.1 ± 0.7) × 10^{-7} s for **1**, **2**, and **3**, respectively.

The Cole−Cole analysis[43] was performed for **2** and **3** using the above ac susceptibilities. We applied the equation $\chi(\omega) = \chi_S + (\chi_T - \chi_S)/(1 + (i\omega\tau)^{1-\alpha})$ where χ_T and χ_S are the isothermal and adiabatic magnetic susceptibilities, respectively.[5c] A semicircle with a small value of α usually indicates one relaxation process operative. Actually, these plots displayed a partial semicircle (Figure S2, ESI), and the optimized α values were 0.32 ± 0.03 at 1.9 K for **2** and 0.16 ± 0.01 at 1.9 K for **3**. The results on ac magnetic susceptibilities are summarized in Table

DOI: 10.1021/acs.inorgchem.5b01583
Inorg. Chem. 2015, 54, 9543−9555

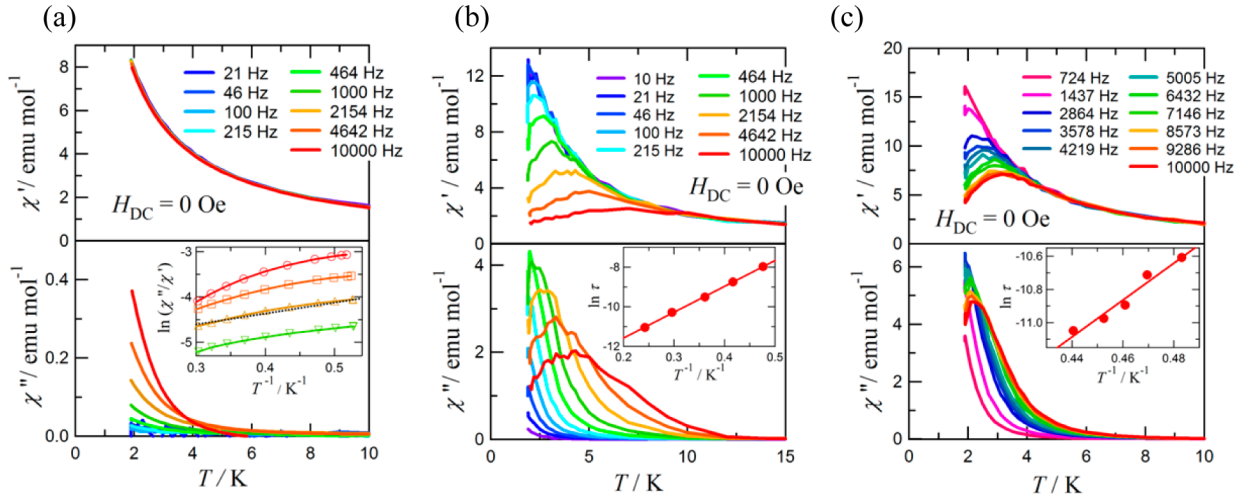

Figure 4. The ac magnetic susceptibilities (in-phase, χ' (top), and out-of-phase, χ'' (bottom)) measured for (a) **1**, (b) **2**, and (c) **3** without any dc bias field. Lines are shown as a guide to the eyes. The insets show the (modified) Arrhenius plots together with optimized lines.

Table 4. Effective Energy Barrier, U_{eff}, Pre-exponential Factor, τ_0, and α in the Cole−Cole Analysis from the ac Magnetic Susceptibility Measurements

	1	2	3
$U_{eff}\ k_B^{-1}$, K	2.4 ± 0.6	13.0 ± 0.2	11 ± 1
τ_0, s	(3.6 ± 0.1) × 10^{-7}	(6.9 ± 0.5) × 10^{-7}	(1.1 ± 0.7) × 10^{-7}
α at 1.9 K	−[a]	0.32 ± 0.03	0.16 ± 0.01

[a]Not determined because of the narrow range of the susceptibility data.

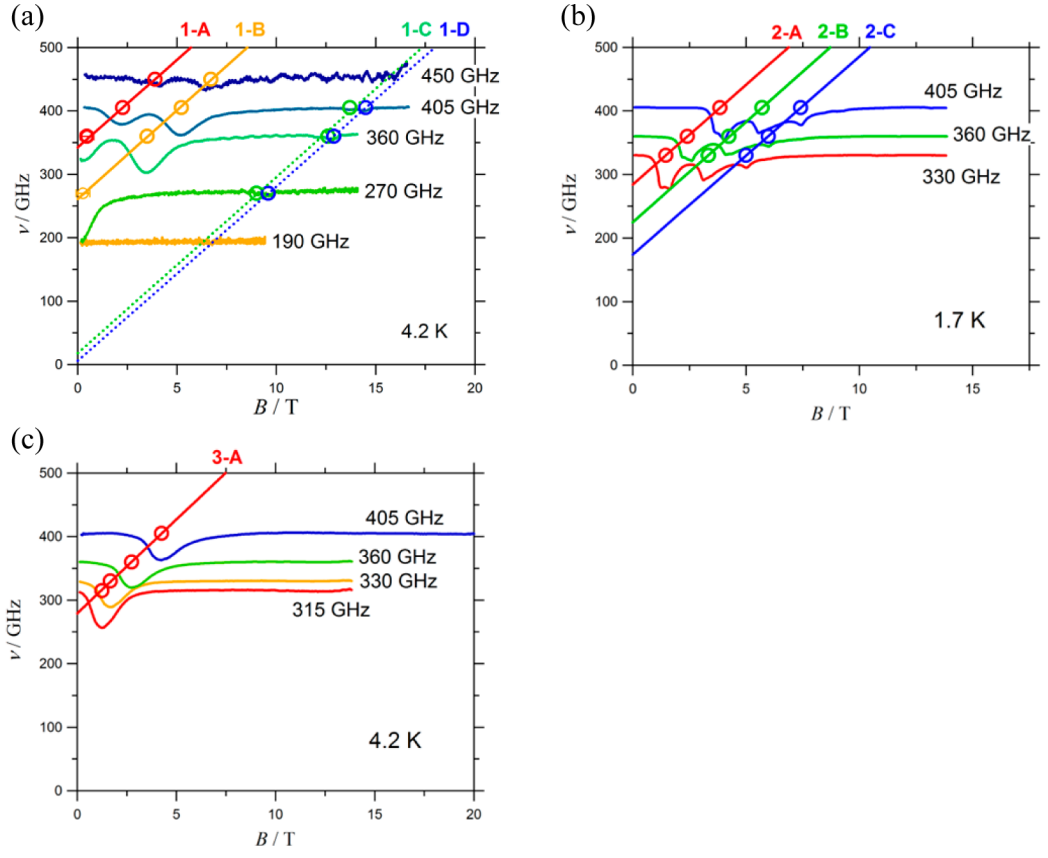

Figure 5. Combined plots of the spectra and the frequency-field relation for (a) **1**, (b) **2**, and (c) **3**. The temperatures are indicated inside the panels. Each spectrum is given an offset corresponding to the frequency. Solid lines are the linear fits of the frequency−field diagrams. Small signals found in **1**, presumably due to impurities, are indicated by the dotted lines.

DOI: 10.1021/acs.inorgchem.5b01583
Inorg. Chem. 2015, 54, 9543−9555

Table 5. HF-EPR Results of 1, 2, and 3

	1		2			3
peak number	1-A	1-B	2-A	2-B	2-C	3-A
g	2.0 ± 0.1	2.00 ± 0.08	2.27 ± 0.04	2.26 ± 0.04	2.26 ± 0.02	2.11 ± 0.04
J^z	±15/2	±11/2	±15/2	±11/2	±9/2	±15/2
J/k_B	2.25 ± 0.05		1.82 ± 0.04			1.79 ± 0.04

4. The presence of the finite barriers supports that the present compounds behave as SMMs.

HF-EPR Study. HF-EPR spectra of a powder specimen were collected in a wide frequency range between 95 and 450 GHz at 4.2 K for **1** and **3** and at 1.7 K for **2** (Figure 5). In the plot, each spectrum is given as the offset corresponding to the frequency, and the resonance fields are also plotted in the same figure. Hence, the figure is the combined plot of the frequency dependence of spectra and the frequency−field relation.

Compound **1** shows two strong absorptions (1-A and 1-B) and a few weak ones (1-C and 1-D), and **2** shows three strong absorptions (2-A, 2-B, and 2-C) with additional doublet structures at each signal, while **3** shows practically only one strong absorption (3-A). The slopes of the EPR modes defined as effective g values are listed in Table 5. All of them fell in the range from 2.0 ± 0.1 to 2.27 ± 0.04. The intensity for all of the EPR absorptions monotonically decreased with increasing temperature (Figure S3, ESI). This finding indicates that the absorption is assigned to the transition from the ground state or low-lying states.

An effective g value in the $J^z = \pm 15/2$ doublets of Dy^{3+} would be 20, which is much different from the observed g values. Hence, the signals can be assigned to a Cu^{2+}-related transition biased with the exchange field between Cu^{2+} and Dy^{3+}. Strictly speaking, the reversal of the Cu^{2+} spin is a forbidden EPR transition because it is associated with the change of the total angular momentum of the exchange coupled effective moment. However, transition becomes observable when the molecular symmetry is low and the different states are mixed. Such conditions may be applicable for the present systems.

Let us explain the procedure of evaluating exchange couplings by using an energy level diagram for the simplest case of **3**. We follow the procedure that has been applied to various systems.[15−17] The outline is as follows: (1) Ln ions are treated as Ising spins. In other words, only the lowest J^z doublet of Dy^{3+} is included. This treatment can be justified when the splitting between the ground and the excited states is larger than the EPR frequencies and the measurement was performed at low temperatures. (2) The energy level diagram was drawn by assuming the sign of 4f−3d exchange coupling and the possible EPR transitions by the reversal of 3d spins are assigned. (3) The magnitude of the exchange coupling is evaluated by adjusting the splittings of the calculated energy levels with those of the experimental data. (4) In case of antiferromagnetic exchange coupling, the level crossing in the energy level diagram is assigned to the magnetization steps. The last procedure is not used in the present case since there is no level crossing for ferromagnetically coupled molecules.

We utilized the following spin-Hamiltonian:

$$H = -J_{Dy-Cu1} J^z_{Dy} \cdot S_{Cu1} - J_{Dy-Cu2} J^z_{Dy} \cdot S_{Cu2} + \mu_B H^z (g_{Dy} J^z_{Dy} + g_{Cu1} S_{Cu1} + g_{Cu2} S_{Cu2}) \quad (3)$$

Here, the first and second terms represent the exchange energy between the Dy^{3+} and two Cu^{2+} spins. The exchange coupling between two terminal Cu1···Cu2 is disregarded because of the long Cu···Cu distance. Owing to the molecular symmetry, the condition of $J_{Dy-Cu1} = J_{Dy-Cu2}$ is applied for **1** and **3**. The third term expresses the Zeeman energies of magnetic ions.

First we analyze the simplest energy level diagram of **3**, depicted in Figure 6. As mentioned previously, the observed

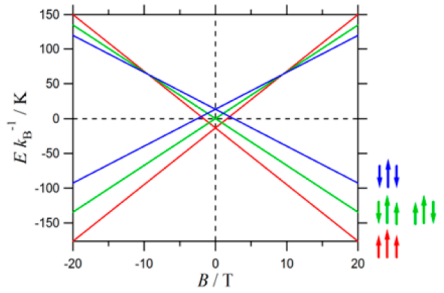

Figure 6. Energy levels of **3** in the ground state $J^z = 15/2$ manifold. The arrangement of Dy (long arrow) and Cu (short arrows) magnetic moments are schematically shown.

EPR signal is the transition from the ground state. Hence, the signal should be assigned to the transition between the red and green levels. Note that the green level is doubly degenerated for the presence of two identical exchange couplings. The difference between the red and green levels is expected to increase linearly with the magnetic field, and the exchange coupling energy can be evaluated from the gap at zero magnetic field. These expected characteristic features are consistent with the experimentally obtained linear frequency−field diagram in Figure 5c. From the extrapolation of the EPR mode, the energy gap (ΔE) at zero field is evaluated to be 279 ± 1 GHz. The J_{Dy-Cu} was derived according to the relation $\Delta E = -2J_{Dy-Cu}(J^z_{Dy} \cdot S_{Cu1})$, from the first term of eq 3. The Dy−Cu exchange coupling, J_{Dy-Cu}, was determined to be $J/k_B = +1.79 \pm 0.04$ K. Here, we use the parameters $S_{Cu1} = S_{Cu2} = 1/2$, $g_{Cu1} = g_{Cu2} = 2.11 \pm 0.04$, $J^z_{Dy} = 15/2$, and $g_{Dy} = 4/3$. The parameters obtained from the HF-EPR experiments are listed in Table 5. The level-crossing field was 9.5 ± 0.2 T (Figure 6), which implies the crossing of two states with respect to the Cu spin-flip and shows degeneracy due to the symmetry. In Figure 5c, the level-crossing field corresponds to the field-axis intercept with the extrapolation of line 3-A. Such a negative crossing field is not detected in magnetization curves when the exchange coupling is ferromagnetic.

Next we analyze the result of **1**. In Figure 5a, two weak absorptions (1-C and 1-D) with $g = (2.0 \pm 0.2 - (1.97 \pm 0.02)$ were found besides the strong peaks. Since the extrapolation of these modes goes to the origin of the frequency−field diagram, we consider these as Cu^{2+}-involved impurity and remove them from further analysis. This content is practically negligible, as guaranteed by the PXRD data (Figure 1 (top)).

The behavior of each of two major absorptions 1-A and 1-B of **1** is quite similar to the signal 3-A for **3**. There are two possible interpretations for the observation of two EPR modes.

DOI: 10.1021/acs.inorgchem.5b01583
Inorg. Chem. 2015, 54, 9543−9555

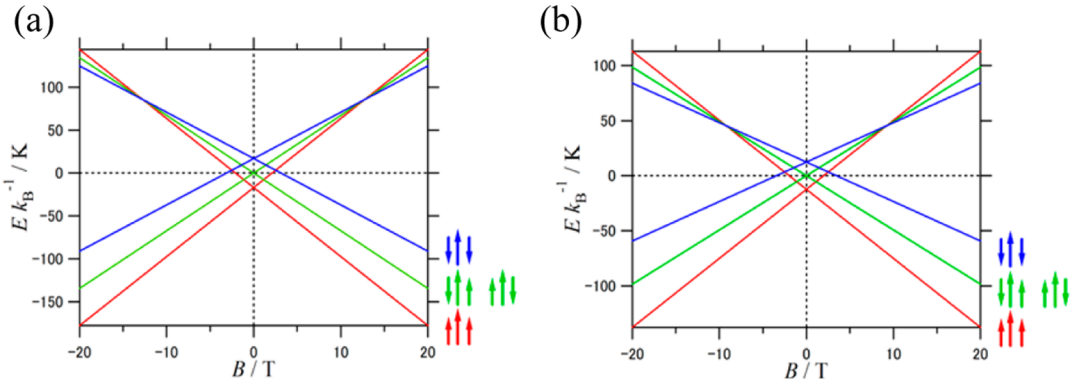

Figure 7. Energy levels of **1** with J^z = 15/2 (a) and J^z = 11/2 (b) for Dy^{3+}. The arrangement of Dy (long arrow) and Cu (short arrows) magnetic moments are schematically shown.

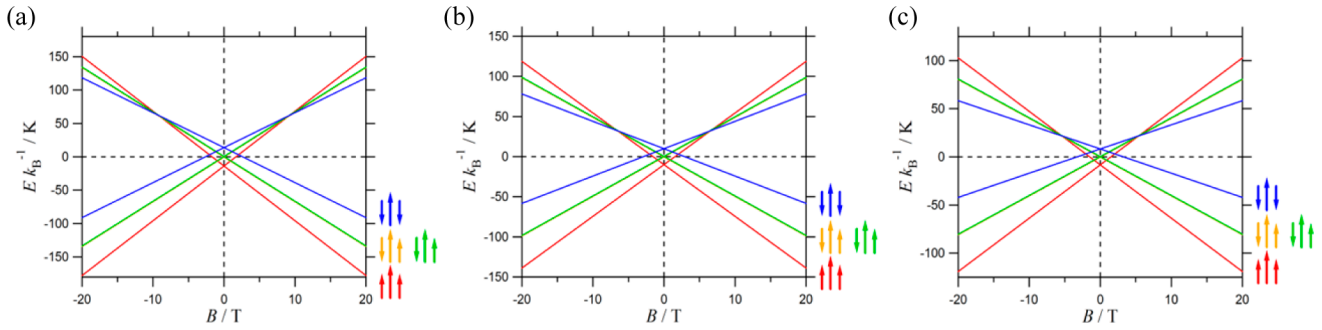

Figure 8. Energy levels of **2** with $J^z = \pm$ 15/2 (a), $J^z = \pm$ 11/2 (b), and $J^z = \pm$ 9/2 (c) for Dy^{3+}. The arrangement of Dy (long arrow) and Cu (short arrows) magnetic moments are schematically shown.

Table 6. Exchange Parameter, J_{Dy-Cu}, for the DyO_2Cu Compounds Determined from the HF-EPR Study and Important Geometrical Parameters

	1	2	3	A[e]	B[f]
$J_{Dy-Cu}k_B^{-1}$, K	2.25 ± 0.05	1.82 ± 0.04	1.79 ± 0.04	1.63 ± 0.01	0.90 ± 0.01
coordination number	10	9	10	10	8
Dy−O,[a] Å	2.370 ± 0.002	2.40 ± 0.06	2.382 ± 0.006	2.367 ± 0.005	2.52 ± 0.03
Cu−O,[a] Å	1.948 ± 0.004	1.95 ± 0.02	1.9755 ± 0.0005	1.957 ± 0.001	1.932 ± 0.003
θ,[b] deg	99.3 ± 0.2	99.8 ± 2.0	100.5 ± 0.2	108.2 ± 0.2	109.5 ± 0.8
ϕ,[c] deg	140.9 ± 0.1	147.1 ± 1.9	142.4 ± 0.2	162.7 ± 0.1	179.1 ± 0.8
d,[d] Å	3.301 ± 0.001	3.33 ± 0.02	3.358 ± 0.001	3.510 ± 0.003	3.65 ± 0.01

[a]The average bond length in the DyO_2Cu unit(s). [b]The average Dy−O−Cu bond angle. [c]The Dy−O···O−Cu butterfly angle. For **2** and **B**, averaged values are applied. [d]The Dy···Cu distance. For **2** and **B**, averaged values are applied. [e]From ref 16. [f]From ref 15.

The first one is the coexistence of two nonequivalent Dy−Cu exchange couplings, or in other words the case of $J_{Dy-Cu1} \neq J_{Dy-Cu2}$. However, this is unlikely for **1**, because the crystallographic analysis clarified that the two Dy−Cu bonds are identical.

An alternative interpretation is that the two signals originate from the admixture of two kinds of J^z doublets of Dy^{3+} ion in the ground-state wave function. According to eq 3, the ratio of the zero-field energy values of two modes should scale with J^z. The ratio of zero-field energy, 261 ± 6 GHz/347 ± 2 GHz = 0.75, is close to the ratio of J^z values, (11/2)/(15/2) = 0.73. The matching of the theoretical and experimental ratios indicates that the second interpretation is more plausible. In 4f-electron systems, the mixing of the J^z states happens in low-symmetry molecules through spin−orbit coupling and CFS. There are some known Dy^{3+} compounds with a ground J^z = ±11/2 state,[44] in which a 2-fold symmetry was characterized like **1**.[45] It also supports that the two EPR modes found in **1** originated from the mixture of two J^z states. The exchange coupling is thus determined to be J_{Dy-Cu}/k_B = 2.25 ± 0.05 K. The determined Zeeman diagrams for J^z_{Dy} = ±15/2 and ±11/2 are shown in Figure 7.

Finally, we move to analyze the data of **2** (Figure 5b). There are two Cu^{2+} sites in the crystal of **2**, and thus $J_{Dy-Cu1} \neq J_{Dy-Cu2}$ could give two modes. However, the number of absorptions is more than expected. The phase purity is assured by the PXRD data (Figure 1 (bottom)). In this case, we have to consider the admixture of the multiple J^z states in the ground state. The zero-field energies of the three groups are 285 ± 6, 225 ± 3, and 174 ± 2 GHz and the ratio is 1/0.79/0.61, being close to the ratio 1/0.73/0.60 from J^z = ±15/2, ±11/2, and ±9/2. Hence, the splitting into three major groups is due to the mixing of three J^z doublets in the ground state, and the small splitting within each group is caused by the nonequivalent Dy−Cu exchange interactions. The almost equal intensity between the two peaks of the each group is consistent with the small

DOI: 10.1021/acs.inorgchem.5b01583
Inorg. Chem. 2015, 54, 9543−9555

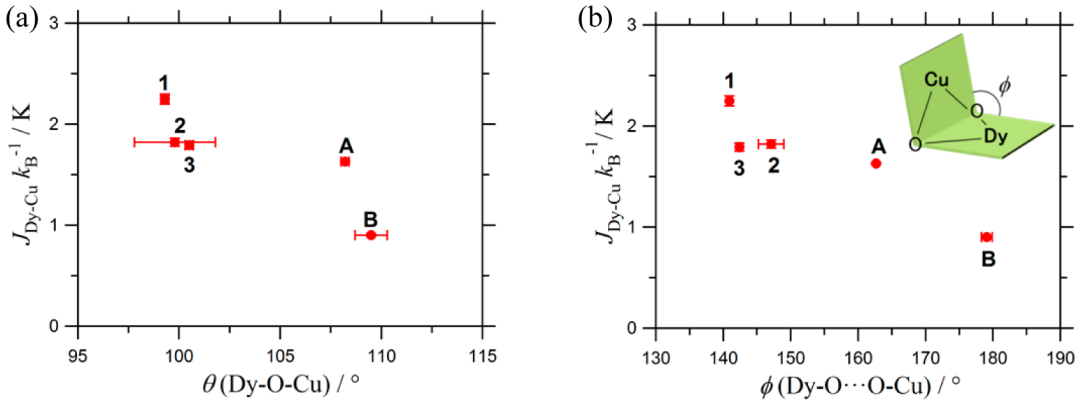

Figure 9. Plots of the Dy−Cu exchange parameters in five DyO_2Cu compounds (a) as a function of θ(Dy−O−Cu) and (b) as a function of ϕ(Dy−O···O−Cu).

variation of the exchange couplings at two independent sites in a unit cell. The g values of the signals were 2.1 ± 0.1 and 2.24 ± 0.04. We have evaluated the two exchange coupling parameters J_{Dy-Cu1}/k_B = 1.87 ± 0.02 K and J_{Dy-Cu2}/k_B = 1.79 ± 0.01 K, which are different from each other by 4%. The zero-field energy of 285 ± 6 GHz is an average value from the two distinct energies. The exchange coupling parameter was determined to J_{Dy-Cu}/k_B = 1.82 ± 0.04 K for **2** (Table 5). The determined Zeeman diagrams for J^z_{Dy} = ±15/2, ±11/2, and ±9/2 are shown in Figure 8.

The HF-EPR analysis elucidated not only the Dy−Cu exchange coupling, but also the mixing of the Dy^{3+} ground-state wave functions. Even a tiny variation of exchange couplings for the nonequivalent bonds can be resolved clearly. Such quantitative and precise determination of the exchange coupling highlights the powerfulness of the HF-EPR.

DISCUSSION

Now let us discuss the magneto−structure relation for the series of Dy−Cu compounds. To expand the parameter survey range, the data of two known compounds, **A** ($[Cu^{II}(L^A)(C_3H_6O)Dy^{III}(NO_3)_3]$; H_2L^A = *N*,*N*′-bis(3-methoxysalicylidene)-1,3-diamino-2,2-dimethylpropane)[16] and **B** ($[Dy^{III}L^B_2(NO_3)_2\{Cu^{II}(CH_3OH)\}_2](NO_3)(CH_3OH)$; H_2L^B = 2,6-bis(acetylaceto)pyridine),[15] with analogous DyO_2Cu structures are included in the discussion. Table 6 summarizes the exchange coupling constants, J_{Dy-Cu}, together with the geometrical parameters. In the following analysis, we used the averaged value of two exchange couplings in **2** and **B**, because of the uncertainty of the assignment of two exchange couplings to two Cu sites. It is found that the exchange coupling of **1** is the largest and twice as large as that of **B**, while the values of **2** and **3** are only slightly larger than that of **A**.

At the first stage, we investigated the relationship between the coordination number (CN) of the Dy^{3+} ion and the Dy−O bond length. Figure S4a (ESI) shows the normalized Dy−O bond length against the CN. The Dy−O bond length of the CN = 8 subset is longer than those of the CN = 10 subset by ca. 6%. It is quite unusual, because in general an increase of CN enlarges the ionic radius.[46] A possible reason for the present anomaly may reside in the rigid coordination structure of **B**, where the Dy^{3+} ion is surrounded by a compartment metalloligand or metallacrown[47] $[L^B_2Cu^{II}_2]$. The resultant structure is highly planar and loses configurational freedom. The Dy−O distance is thus regulated by the $[L^B_2Cu^{II}_2]$ structure itself regardless of CN. Discussion using CN requires special attention.

Next, we plotted the exchange coupling against the bond lengths of Dy−O and Cu−O averaged in the DyO_2Cu core structure, as shown in Figure S4b (ESI). Compound **1** has O5 at an axial position of Cu1, and **2** also has O3 at an axial site of Cu1 (see above). The contribution of the Dy1−O(axial)−Cu1 pathways is negligible. The exchange coupling is insensitive to the Cu−O bond lengths but seems to depend slightly on the Dy−O bond lengths. Compound **B** with the longest Dy−O distance gives the weakest exchange coupling. Another relation between the exchange coupling and the Dy···Cu interatomic distance (Figure S5, ESI) also exhibits that shorter distance favors stronger exchange coupling.

The plot of exchange coupling against the Dy−O−Cu bond angle is shown in Figure 9a. The angle is the average of the double oxygen paths. We found that the bond angles are split into two regimes around 100° and 109°. The average of exchange couplings of the three samples in the former regime is larger than the average in the latter regime. As a general trend of the Gd−Cu case, the exchange coupling decreases with increasing Gd−O−Cu bond angles, while exchange coupling does not much depend on the Cu−O bond length.[13,48] In the framework of the superexchange mechanism, the exchange coupling between Dy and Cu depends on the orbital overlap and the orthogonality in the Dy−O−Cu bond. The Dy−O−Cu angle may have a clue to the exchange coupling mechanism. At the present stage, however, cautious analysis is needed for further discussion because of the narrow range of the bond angles.

Finally, we discuss the effect of the geometrical parameter governing the skeleton of the molecule. In Figure S5 (ESI), we have plotted the exchange parameter against the Dy···Cu distance. Since the Dy···Cu distance becomes shorter when the Dy−O−Cu bond angle is smaller, the plot is related to Figure 9a. Furthermore, the plot of the exchange parameter vs the Dy−O bond length shown in Figure S4b (ESI) is also related to Figure 9a. As already mentioned, the bridge using the Cu axial site is useless for the exchange coupling. However, such an axial bridge may play an important role for the molecular skeleton; for example, it would force the Cu−O−Dy angles narrower and the Cu−O···O−Dy dihedral angle smaller, as found in **1** and **2**.

As cited above, it is well-known that J_{Gd-Cu} value shows a relation with the butterfly angle ϕ.[11−13] The largest J/k_B = 18.1 K was characterized for ϕ = 178.39° and a smaller J/k_B = 0.6 K was obtained for ϕ = 147.01°. A general trend in the relation

DOI: 10.1021/acs.inorgchem.5b01583
Inorg. Chem. 2015, 54, 9543−9555

between J_{Dy-Cu} and ϕ is also recognized, but the profile is quite different (Figure 9b). This trend may be understood in two ways. First, the change of ϕ causes the change of the Dy−O−Cu bond angle. Another possibility is that the overlap or orthogonality of the Dy−O−Cu bond varies with ϕ. These two can be understood by considering the change of bonding with spatial extension and direction of lanthanide wave functions.

Although the exchange coupling must be related to the local structure of each bond; namely, the bond lengths and the bond angles, the butterfly angle may be useful to discuss the whole DyO_2Cu skeleton of the molecule holding the larger exchange couplings. Further investigation combined with quantum chemistry calculation may unveil the underlying rule of magneto−structure relation and the mechanism of the strong 4f−3d exchange coupling.

CONCLUSION

We have synthesized three new Dy−Cu SMMs with large ferromagnetic exchange coupling after paying attention to the structural diversity of hinge-like coordination flexibility. We clarified the following: (1) New molecular structures can be obtained by the control of solvents. (2) The strong exchange couplings are caused by the double bridge structure. (3) HF-EPR is a unique method to determine the exchange coupling and the state of the rare earth ions, affording the J_{Dy-Cu} values in the (1.79 ± 0.04)−(2.25 ± 0.05) K for **1**−**3**. (4) By examination of the structural parameters in three present and two additional known compounds, the relations between the exchange couplings and bond angles and butterfly angles is found. The butterfly angle representing the DyO_2Cu skeleton is a simple but a useful parameter to predict the strength of exchange couplings.

The present work gives the first detailed investigation of magneto−structure relation based on the precise determination of exchange coupling in Dy−Cu compounds. Such relationship allows us to draw molecular design and improve the magnetic exchange coupling in various molecule-based magnets, including cubane and semicubane structures often found in SMMs. Moreover, doubly oxygen-bridged motifs are commonly found in metal oxides, so that the present compounds might be regarded as minimum exchange-coupled models or prototypes for polymeric oxide-based magnets. Although the explanation has to wait for theoretical treatment, empirical magneto−structural relation will be applied to design 4f−3d-based magnetic materials. The established methodology will make great progress in the study of the exchange coupling mechanism in heterometallic complexes.

ASSOCIATED CONTENT

Supporting Information

The Supporting Information is available free of charge on the ACS Publications website at DOI: 10.1021/acs.inorgchem.5b01583.

Bond distances and bond angles around the metal ions in **1**−**3**, *M-H* curves of powder **1**, **2**, and **3**, Cole−Cole plot for **2** and **3**, variable temperature HF-EPR, and possible magneto−structure relations (PDF)

Crystallographic information for **1**, CCDC 1059357 (CIF)

Crystallographic information for **2**, CCDC 1059358 (CIF)

Crystallographic information for **3**, CCDC 1050447 (CIF)

AUTHOR INFORMATION

Corresponding Authors

*E-mail: ishi@pc.uec.ac.jp (T. I.).
*E-mail: nojiri@imr.tohoku.ac.jp (H. N.).
*E-mail: ghosh_59@yahoo.com (A. G.).

Author Contributions

⊥Ms. Yumi Ida and Mr. Soumavo Ghosh equally contributed to this work.

Notes

The authors declare no competing financial interest.

ACKNOWLEDGMENTS

A part of this work was performed under the Interuniversity Cooperative Research Program of the Institute for Materials Research, Tohoku University (Proposal Nos. 13K0089, 14K0047, and 15K0022). T. I. thanks financial support from KAKENHI (JSPS/15H03793). A. G. thanks the Department of Science and Technology (DST), New Delhi, India, for financial support (SR/S1/IC/0034/2012) as well as the DST-FIST funded single crystal X-ray diffractometer facility at the Department of Chemistry, University of Calcutta. S. G. is thankful to the University Grants Commission (UGC), New Delhi for Senior Research Fellowship. We are also thankful to Prof. Michael G. B. Drew, School of Chemistry, University of Reading, for discussion on crystal structural solutions.

REFERENCES

(1) Osa, S.; Kido, T.; Matsumoto, N.; Re, N.; Pochaba, A.; Mrozinski, J. *J. Am. Chem. Soc.* **2004**, *126*, 420−421.

(2) (a) Mori, F.; Nyui, T.; Ishida, T.; Nogami, T.; Choi, K.-Y.; Nojiri, H. *J. Am. Chem. Soc.* **2006**, *128*, 1440−1441. (b) Ueki, S.; Ishida, T.; Nogami, T.; Choi, K.-Y.; Nojiri, H. *Chem. Phys. Lett.* **2007**, *440*, 263−267.

(3) Pointillart, F.; Bernot, K.; Sessoli, R.; Gatteschi, D. *Chem. - Eur. J.* **2007**, *13*, 1602−1609.

(4) Ishikawa, N.; Sugita, M.; Ishikawa, T.; Koshihara, S.-y.; Kaizu, Y. *J. Am. Chem. Soc.* **2003**, *125*, 8694−8695.

(5) (a) Rinehart, J. D.; Long, J. R. *Chem. Sci.* **2011**, *2*, 2078−2085. (b) Woodruff, D. N.; Winpenny, W. R. E. P.; Layfield, R. A. *Chem. Rev.* **2013**, *113*, 5110−5148. (c) Sessoli, R.; Powell, A. K. *Coord. Chem. Rev.* **2009**, *253*, 2328−2341. (d) Andruh, M.; Costes, J. P.; Diaz, C.; Gao, S. *Inorg. Chem.* **2009**, *48*, 3342−3359. (e) Lin, P. H.; Burchell, T. J.; Ungur, L.; Chibotaru, L. F.; Wernsdorfer, W.; Murugesu, M. *Angew. Chem., Int. Ed.* **2009**, *48*, 9489−9492. (f) Rinehart, J. D.; Fang, M.; Evans, W. J.; Long, J. R. *Nat. Chem.* **2011**, *3*, 538−542. (g) Feltham, H. L. C.; Brooker, S. *Coord. Chem. Rev.* **2014**, *276*, 1−33. (h) Zhang, P.; Zhang, L.; Wang, C.; Xue, S. F.; Lin, S. Y.; Tang, J. K. *J. Am. Chem. Soc.* **2014**, *136*, 4484−4487.

(6) Yamauchi, S.; Fujinami, T.; Matsumoto, N.; Mochida, N.; Ishida, T.; Sunatsuki, Y.; Watanabe, M.; Tsuchimoto, M.; Coletti, C.; Re, N. *Inorg. Chem.* **2014**, *53*, 5961−5971.

(7) (a) Bencini, A.; Benelli, C.; Caneschi, A.; Carlin, R. I.; Dei, A.; Gatteschi, D. *J. Am. Chem. Soc.* **1985**, *107*, 8128−8136. (b) Matsumoto, N.; Sakamoto, M.; Tamaki, H.; Okawa, H.; Kida, S. *Chem. Lett.* **1990**, *19*, 853−854. (c) Guillou, O.; Bergerat, P.; Kahn, O.; Bakalbassis, E.; Boubekeur, K.; Batail, P.; Guillot, M. *Inorg. Chem.* **1992**, *31*, 110−114.

(8) Andruh, M.; Ramade, I.; Codjovi, E.; Guillou, O.; Kahn, O.; Trombe, J. C. *J. Am. Chem. Soc.* **1993**, *115*, 1822−1829.

(9) (a) Costes, J.-P.; Dahan, F.; Dupuis, A. *Inorg. Chem.* **2000**, *39*, 5994−6000. (b) Costes, J.-P.; Dahan, F.; Dupuis, A.; Laurent, J.-P. *Inorg. Chem.* **2000**, *39*, 169−173. (c) Costes, J.-P.; Dahan, F.; Dupuis, A.; Laurent, J.-P. *Chem. - Eur. J.* **1998**, *4*, 1616−1620.

DOI: 10.1021/acs.inorgchem.5b01583
Inorg. Chem. 2015, 54, 9543−9555

(10) (a) Kido, T.; Ikuta, Y.; Sunatsuki, Y.; Ogawa, Y.; Matsumoto, N.; Re, N. *Inorg. Chem.* **2003**, *42*, 398−408. (b) Evangelisti, M.; Kahn, M. L.; Bartolome, J.; de Jongh, L. J.; Meyers, C.; Leandri, J.; Leroyer, Y.; Mathoniere, C. *Phys. Rev. B: Condens. Matter Mater. Phys.* **2003**, *68*, 184405.
(11) Costes, J.-P.; Dahan, F.; Dupuis, A. *Inorg. Chem.* **2000**, *39*, 165−168.
(12) Ramade, I.; Kahn, O.; Jeannin, Y.; Robert, F. *Inorg. Chem.* **1997**, *36*, 930−936.
(13) Ryazanov, M.; Nikiforov, V.; Lloret, F.; Julve, M.; Kuzmina, N.; Gleizes, A. *Inorg. Chem.* **2002**, *41*, 1816−1823.
(14) (a) Okazawa, A.; Nogami, T.; Nojiri, H.; Ishida, T. *Chem. Mater.* **2008**, *20*, 3110−3119. (b) Baker, M. L.; Tanaka, T.; Murakami, R.; Ohira-Kawamura, S.; Nakajima, K.; Ishida, T.; Nojiri, H. *Inorg. Chem.* **2015**, *54*, 5732−5738.
(15) Shimada, T.; Okazawa, A.; Kojima, N.; Yoshii, S.; Nojiri, H.; Ishida, T. *Inorg. Chem.* **2011**, *50*, 10555−10557.
(16) Ishida, T.; Watanabe, R.; Fujiwara, K.; Okazawa, A.; Kojima, N.; Tanaka, G.; Yoshii, S.; Nojiri, H. *Dalton Trans.* **2012**, *41*, 13609−13619.
(17) (a) Ueki, S.; Okazawa, A.; Ishida, T.; Nogami, T.; Nojiri, H. *Polyhedron* **2007**, *26*, 1970−1976. (b) Okazawa, A.; Nogami, T.; Nojiri, H.; Ishida, T. *Inorg. Chem.* **2008**, *47*, 9763−9765. (c) Okazawa, A.; Nogami, T.; Nojiri, H.; Ishida, T. *Inorg. Chem.* **2009**, *48*, 3292−3292. (d) Okazawa, A.; Watanabe, R.; Nojiri, H.; Nogami, T.; Ishida, T. *Polyhedron* **2009**, *28*, 1808−1813. (e) Okazawa, A.; Watanabe, R.; Nezu, M.; Shimada, T.; Yoshii, S.; Nojiri, H.; Ishida, T. *Chem. Lett.* **2010**, *39*, 1331−1332. (f) Okazawa, A.; Fujiwara, K.; Watanabe, R.; Kojima, N.; Yoshii, S.; Nojiri, H.; Ishida, T. *Polyhedron* **2011**, *30*, 3121−3126. (g) Watanabe, R.; Fujiwara, K.; Okazawa, A.; Tanaka, G.; Yoshii, S.; Nojiri, H.; Ishida, T. *Chem. Commun.* **2011**, *47*, 2110−2112. (h) Fujiwara, K.; Okazawa, A.; Tanaka, G.; Yoshii, S.; Nojiri, H.; Ishida, T. *Chem. Phys. Lett.* **2012**, *530*, 49−54. (i) Okazawa, A.; Shimada, T.; Kojima, N.; Yoshii, S.; Nojiri, H.; Ishida, T. *Inorg. Chem.* **2013**, *52*, 13351−13355.
(18) Kajiwara, T.; Nakano, M.; Takaishi, S.; Yamashita, M. *Inorg. Chem.* **2008**, *47*, 8604−8606.
(19) (a) Liu, K.; Shi, W.; Cheng, P. *Coord. Chem. Rev.* **2015**, *289*−*290*, 74−122. (b) Rosado Piquer, L.; Sañudo, E. C. *Dalton Trans.* **2015**, *44*, 8771−8780.
(20) (a) Das, L. K.; Park, S.-W.; Cho, S. J.; Ghosh, A. *Dalton Trans.* **2012**, *41*, 11009−11017. (b) Ghosh, S.; Aromí, G.; Gamez, P.; Ghosh, A. *Eur. J. Inorg. Chem.* **2014**, *2014*, 3341−3349. (c) Hazari, A.; Das, L. K.; Bauzá, A.; Frontera, A.; Ghosh, A. *Dalton Trans.* **2014**, *43*, 8007−8015. (d) Hazari, A.; Kanta Das, L.; Kadam, R. M.; Bauzá, A.; Frontera, A.; Ghosh, A. *Dalton Trans.* **2015**, *44*, 3862−3876. (e) Das, L. K.; Gómez-García, C. J.; Ghosh, A. *Dalton Trans.* **2015**, *44*, 1292−1302.
(21) Ghosh, S.; Mukherjee, S.; Seth, P.; Mukherjee, P. S.; Ghosh, A. *Dalton. Trans.* **2013**, *42*, 13554−13564.
(22) (a) Ghosh, S.; Ida, Y.; Ishida, T.; Ghosh, A. *Cryst. Growth Des.* **2014**, *14*, 2588−2598. (b) Bencini, A.; Benelli, C.; Caneschi, A.; Carlin, R. L.; Dei, A.; Gatteschi, D. *J. Am. Chem. Soc.* **1985**, *107*, 8128−8136. (c) Harrison, D. W.; Bünzli, J.-C. G. *Inorg. Chim. Acta* **1985**, *109*, 185−192. (d) Bencini, A.; Benelli, C.; Caneschi, A.; Dei, A.; Gatteschi, D. *Inorg. Chem.* **1986**, *25*, 572−575. (e) Ghosh, S.; Biswas, S.; Bauza, A.; Barcelo-Oliver, M.; Frontera, A.; Ghosh, A. *Inorg. Chem.* **2013**, *52*, 7508−7523.
(23) (a) Drew, M. G. B.; Prasad, R. N.; Sharma, R. P. *Acta Crystallogr., Sect. C: Cryst. Struct. Commun.* **1985**, *41*, 1755−1758. (b) Ghosh, S.; Aromí, G.; Gamez, P.; Ghosh, A. *Eur. J. Inorg. Chem.* **2015**, *2015*, 3028−3037.
(24) Sheldrick, G. M. *SHELXS 97 Program for Structure Solution*; University of Göttingen: Germany, 1997.
(25) Sheldrick, G. M. *SHELXL 97 Program for Crystal Structure Refinement*; University of Göttingen: Germany, 1997.
(26) *SAINT*, version 6.02; *SADABS*, version 2.03; Bruker AXS, Inc.: Madison, WI, 2002.
(27) Spek, A. L. *J. Appl. Crystallogr.* **2003**, *36*, 7−13.
(28) Farrugia, L. J. *J. Appl. Crystallogr.* **1997**, *30*, 565−565.
(29) Farrugia, L. J. *J. Appl. Crystallogr.* **1999**, *32*, 837−838.
(30) Kahn, O. *Molecular Magnetism*; VCH: Weinheim, Germany, 1993; Chapter 1, Table I.1.
(31) Nojiri, H.; Ajiro, Y.; Asano, T.; Boucher, J.-P. *New J. Phys.* **2006**, *8*, 218.
(32) (a) Nakamoto, K. *Infrared and Raman Spectra of Inorganic and Coordination Compounds*, 4th ed.; Wiley: New York, 1986. (b) Bullock, J. I. *J. Inorg. Nucl. Chem.* **1967**, *29*, 2257−2264.
(33) Addison, A. W.; Rao, T. N.; Reedijk, J.; Van Rijn, J.; Verschoor, G. C. *J. Chem. Soc., Dalton Trans.* **1984**, 1349−1356.
(34) Ruiz-Martínez, A.; Alvarez, S. *Chem. - Eur. J.* **2009**, *15*, 7470−7480.
(35) (a) Costes, J.-P.; Dahan, F.; Dupuis, A.; Laurent, J.-P. *New J. Chem.* **1998**, *22*, 1525−1529. (b) Novitchi, G.; Shova, S.; Caneschi, A.; Costes, J. P.; Gdaniec, M.; Stanica, N. *Dalton Trans.* **2004**, 1194−1200. (c) Bi, W.; Wei, T.; Lü, X.-Q.; Hui, Y.; Song, J.; Zhao, S.; Wong, W.-K.; Jones, R. A. *New J. Chem.* **2009**, *33*, 2326−2334. (d) Miao, T.-Z.; Feng, W.-X.; Zhang, Z.; Su, P.-Y.; Lü, X.-Q.; Song, J.-R.; Fan, D.-D.; Wong, W.-K.; Jones, R. A.; Su, C.-Y. *Eur. J. Inorg. Chem.* **2014**, *2014*, 2839−2848.
(36) (a) Wang, H.; Zhang, D.; Ni, Z.-H.; Li, X.; Tian, L.; Jiang, J. *Inorg. Chem.* **2009**, *48*, 5946−5956. (b) Zhou, Q.; Yang, F.; Liu, D.; Peng, Y.; Li, G.; Shi, Z.; Feng, S. *Dalton Trans.* **2013**, *42*, 1039−1046.
(37) Andruh, M. *Chem. Commun.* **2011**, *47*, 3025−3042.
(38) Shiga, T.; Ohba, M.; Ōkawa, H. *Inorg. Chem.* **2004**, *43*, 4435−4446.
(39) (a) Tudor, V.; Kravtsov, V.; Julve, M.; Lloret, F.; Simonov, Y. A.; Lipkowski, J.; Buculei, V.; Andruh, M. *Polyhedron* **2001**, *20*, 3033−3037. (b) Bellini, V.; Lorusso, G.; Candini, A.; Wernsdorfer, W.; Faust, T. B.; Timco, G. A.; Winpenny, R. E. P.; Affronte, M. *Phys. Rev. Lett.* **2011**, *106*, 227205. (c) Castro, I.; Sletten, J.; Calatayud, M. L.; JuIve, M.; Cano, J.; Lloret, F.; Caneschi, A. *Inorg. Chem.* **1995**, *34*, 4903−4909.
(40) (a) Kahn, M. L.; Mathoniere, C.; Kahn, O. *Inorg. Chem.* **1999**, *38*, 3692−3697. (b) Towatari, M.; Nishi, K.; Fujinami, T.; Matsumoto, N.; Sunatsuki, Y.; Kojima, M.; Mochida, N.; Ishida, T.; Re, N.; Mrozinski, J. *Inorg. Chem.* **2013**, *52*, 6160−6178.
(41) (a) Sessoli, R.; Tsai, H.-L.; Schake, A. R.; Wang, S.; Vincent, J. B.; Folting, K.; Gatteschi, D.; Christou, G.; Hendrickson, D. N. *J. Am. Chem. Soc.* **1993**, *115*, 1804−1816. (b) Gatteschi, D.; Sessoli, R.; Villain, J. *Molecular Nanomagnets*; Oxford University Press: New York, 2006.
(42) Bartolomé, J.; Filoti, G.; Kuncser, V.; Schinteie, G.; Mereacre, V.; Anson, C. E.; Powell, A. K.; Prodius, D.; Turta, C. *Phys. Rev. B: Condens. Matter Mater. Phys.* **2009**, *80*, 014430.
(43) Cole, K. S.; Cole, H. R. *J. Chem. Phys.* **1941**, *9*, 341−352.
(44) (a) Ritchie, C.; Speldrich, M.; Gable, R.-W.; Sorace, L.; Kögerler, P.; Boskovic, C. *Inorg. Chem.* **2011**, *50*, 7004−7014. (b) Al Damen, M. A.; Cardona-Serra, S.; Clemente-Juan, J. M.; Coronado, E.; Gaita-Ariño, A.; Marti-Gastaldo, C.; Luis, F.; Montero, O. *Inorg. Chem.* **2009**, *48*, 3467−3479.
(45) Lucaccini, E.; Sorace, L.; Perfetti, M.; Costes, J.-P.; Sessoli, R. *Chem. Commun.* **2014**, *50*, 1648−1651.
(46) (a) Shannon, R. D.; Prewitt, C. T. *Acta Crystallogr., Sect. B: Struct. Crystallogr. Cryst. Chem.* **1969**, *25*, 925−946. (b) Shannon, R. D. *Acta Crystallogr., Sect. A: Cryst. Phys., Diffr., Theor. Gen. Crystallogr.* **1976**, *32*, 751−767.
(47) Mezei, G.; Zaleski, C. M.; Pecoraro, V. L. *Chem. Rev.* **2007**, *107*, 4933−5003.
(48) Cirera, J.; Ruiz, E. *C. R. Chim.* **2008**, *11*, 1227−1234.

DOI: 10.1021/acs.inorgchem.5b01583
Inorg. Chem. 2015, 54, 9543−9555